Rotational energy transfer in OH ($A\ ^2\Sigma^+$, $v'=0$): A method for the direct determination of state-to-state transfer coefficients

Andreas Jörg, Ulrich Meier, and Katharina Kohse-Höinghaus
DLR-Institut für Physikalische Chemie der Verbrennung, D-7000 Stuttgart 80, Federal Republic of Germany

(Received 23 April 1990; accepted 13 July 1990)

We have determined state-to-state rate coefficients for rotational and fine structure transitions of OH ($A\ ^2\Sigma^+$, $v'=0$) in thermal collisions with He and Ar at 300 K. The temporal evolution of single fluorescence lines within the A–X, 0–0 band of OH were measured, exciting either the $F_2(4)$ or $F_2(5)$ state by a nanosecond laser pulse. The OH radical was produced in a discharge flow cell, containing predominantly He or Ar, at various pressures between 1 and 6 mbar. The time resolution in the experimental setup was sufficient to evaluate the rotational energy transfer coefficients directly from the time dependence of two fluorescence lines. The observed average rate coefficients for collisions of OH (A, $v'=0$) with Ar are approximately 3 times larger than those with He. The two rare gases show different qualitative behavior. Whereas the almost isoenergetic transitions with $\Delta J=1$ and $\Delta N=0$ are favored in collisions with Ar, those with $\Delta J=\Delta N=-2$ are favored in collisions with He. In addition, a strong preference for transitions conserving the parity of the OH, a propensity rule, previously reported for rotational relaxation in the A state of OH, was found for collisions with He but not for collisions with Ar. Our experimental results for He and for Ar are in good agreement with recent quantum mechanical calculations of the energy transfer coefficients.

I. INTRODUCTION

The OH radical is an important reactive intermediate in combustion processes. Beside its significance for the understanding of the chemical kinetics of flames, OH is also used as an indicator for the location of flame fronts and for temperature measurements. The technique of laser-induced fluorescence (LIF) is widely applied for the determination of relative or absolute OH number densities.[1] One of the key problems associated with quantitative LIF measurements is collision-induced energy transfer.[2] These processes comprise electronic quenching, vibrational, and rotational relaxation. Whereas a significant number of studies exist which measure the electronic quenching of OH ($A\ ^2\Sigma^+$, $v'=0$)—see Ref. 3 and references therein—little is known about the rotational relaxation within this state. Because of the energy difference between the $v'=0$ and $v'=1$ vibrational levels in the A state of OH, collision-induced $0\rightarrow1$ vibrational excitation is negligible at room temperature and of little importance at flame temperatures. For these reasons we focus our interest primarily on the rotational energy transfer (RET) of OH ($A\ ^2\Sigma^+$, $v'=0$).

Note that RET is used in this publication for all inelastic processes within one vibrational level of a specific electronic state. This means that in case the spin and/or the electronic angular momentum is different from zero, a RET transition is inelastic with respect to the rotational state of the molecule and/or the fine structure level. For example, an $F_2(4)\rightarrow F_1(4)$ transition within a $^2\Sigma$ state is a RET process in this sense, although the rotational state of the molecule remains unchanged during the transition.

LIF is the most convenient method for measurements of state-resolved RET coefficients in electronically excited molecular states. It was first applied in 1971 to Na_2 ($B\ ^1\pi$)[4] and I_2 ($B\ ^3\pi$).[5] Since then, the LIF technique has been utilized to measure the RET in OH ($A\ ^2\Sigma$),[6] Na_2 ($A\ ^1\Sigma$),[7] Li_2 ($A\ ^1\Sigma$),[8] CdH ($A\ ^2\pi$),[9] KH ($A\ ^1\Sigma$),[10] ZnH ($A\ ^2\pi$),[11] CsH ($A\ ^1\Sigma$),[12] CaF ($A\ ^2\pi$),[13] and IF ($B\ ^3\pi$).[14] In all these studies the probabilities for collision-induced RET are evaluated from fluorescence spectra without time resolution. The data analysis was usually performed assuming in a first approximation that only one collision occurs on the average during the lifetime of the excited state. The magnitude of corrections caused by successive collisions in these experiments is determined by the natural lifetime of the excited state, the energy transfer coefficients, and the number density of the collision partner. Assuming a given set of energy transfer coefficients, the importance of these corrections for multiple collisions increases with the natural lifetime of the excited molecule and the number density of the collider. Because the lowest possible pressure is experimentally limited by the S/N ratio of the LIF signal, the multiple collision correction is a serious problem for collisions involving the A state of OH, where the natural lifetime ($\approx$700 ns) is comparatively long.

In addition to LIF, various optical pump/probe techniques utilizing two or more lasers are widely used for the investigation of RET. These techniques have been mainly applied to study inelastic collisions within vibrationally excited levels of molecules in their electronic ground state. For example, the RET of diatomic molecules—HF [$v=1$,[15] $v=2$ (Ref. 16)], NO ($v=2$),[17] H_2 ($v=1$),[18,19] D_2 ($v=1$),[18] HD ($v=1$),[20] and HCl ($v=1$)[21]—have been studied. In a few cases pump/probe techniques were also used to examine the RET in an electronically excited state, e.g., NO (A)[22] and IF ($B\ ^3\pi$).[23] In contrast to the

 0021-9606/90/216453-10$03.00

RET measurements using LIF,[4–14] these pump/probe experiments yield time-resolved information of state-specific populations. For this reason, the experimental information of the pump/probe studies[15–23] is, in principle, similar to the information from the time-resolved LIF experiments presented in this work. However, the data analysis procedure described below is different from those used in pump/probe experiments and should be treated as an alternative to the existing methods.

The RET in the A state of OH was first studied in 1959 by Carrington.[24] Although several groups have subsequently worked in this field,[6,25–29] the only experimental work to date reporting quantitative state-to-state RET coefficients for OH (A) is that of Lengel and Crosley.[6] They applied the LIF technique to study rotational relaxation of OH (A, $v' = 0$) in thermal collisions with N_2, H_2, and Ar. Their data analysis, in which they derive rate coefficients from temporally integrated fluorescence signals, includes an iterative procedure to account for multiple collisions.

We demonstrate here a direct method to determine state-to-state RET coefficients for OH (A). This becomes possible by using improved time resolution, which in our case is determined by the detection apparatus and not by the lifetime of OH (A). The state-to-state RET coefficients are determined from temporal evolution of relative number densities in a laser-pumped state and a state populated by collisions. The relative number densities are easily obtained from LIF signals, using the well-known Einstein coefficients for spontaneous emission.[30] The ratios of these Einstein coefficients are the only molecular constants to which our method is sensitive; in particular, the data analysis is insensitive to the natural lifetimes of the excited states. In a first set of experiments we have applied this method to determine state-to-state rate coefficients for inelastic collisions of OH (A, $v' = 0$) with He and Ar.

Both systems, OH (A) + He and OH (A) + Ar, are of interest because they allow a direct comparison between theoretically and experimentally determined data. For the OH–Ar system, the X and A potential energy surfaces and RET in the A state have been studied[31] using accurate quantum-mechanical methods. In addition, these potential energy surfaces have been used to calculate the bound rovibrational states of the OH (A) + Ar (^1S) van der Waals complex in the gas phase,[32] which has been recently observed by experimental studies.[33] For the OH-He system, quantum scattering calculations of RET in the A state were performed[34] following closely the treatment of OH + Ar.[31] The dynamical calculations for both systems can be compared directly to measurements of the collision-induced RET (Ref. 6 and this work). Results of another theoretical study of the X and A potential energy surfaces[35] and the RET[36] of the OH-He system cannot be directly compared with experimental data due to the limited range of collision energies studied in Ref. 36.

Our long-term goal is to build up a numerical model—based upon state-specific rate equations for laser- and collision-induced processes—to examine the applicability of OH LIF measurements to various combustion environments. Since it is not feasible to measure a complete set of state-specific energy transfer coefficients as a function of collision partner and temperature, we focus our interest on experiments aiming at a better understanding of the various RET processes themselves. The comparison of experimental and theoretical results, which is possible for the OH (A) + He and Ar systems, is important for the interpretation of RET processes. With regard to combustion systems, we have measured coefficients for the rotational relaxation of OH (A, $v' = 0$) with N_2, CO_2, and H_2O.[37] RET measurements for OH (A, $v' = 1$) are planned in the near future because of the interest gained recently in exciting this state for LIF measurements in flames.[38] In addition, the validity of various scaling and fitting laws[39] to describe the RET in OH (A) will be tested. For this, measurements of the upward RET starting from the $F_1(0)$ level are in progress. Transitions involving this lowest rotational level are important for dynamically based scaling laws.

II. EXPERIMENT

The $S_1(2)$ or $S_1(3)$ line of the OH (A–X, 0–0) band was excited with a Nd:YAG pumped, frequency-doubled dye laser. The spectral bandwidth, pulse duration, and pulse energy of the uv radiation were 2 cm^{-1} (FWHM), 5 ns (FWHM), and typically 6–7 mJ/pulse, respectively. The spectral bandwidth of the laser was large compared to the Doppler width of OH at 300 K, therefore no velocity selection occurred during the excitation. For all RET measurements, the polarization of the uv laser radiation was completely scrambled. The use of a polarization scrambler was necessary to generate spatially isotropic LIF signals (see Sec. IV A). The uv beam was unfocused (diameter $\approx$8 mm) in order to avoid diffusional loss of excited OH radicals out of the detection volume during the lifetime of the A state.

The OH was produced by the chemical reaction of NO_2 with H atoms in a discharge flow cell (1–4 SLM) at pressures between 1 and 6 mbar. The H atoms were generated by a microwave discharge through H_2 in He or Ar as carrier gas. The discharge was located at the upstream end of a quartz flow tube (30 cm length and 3 cm internal diameter, treated with HF). The NO_2 was added downstream through a movable inlet. The position of the inlet was optimized to yield the maximum number density for OH in the volume excited by the laser beam. The details of the flow system are described elsewhere.[40] The sum of the partial flows of H_2 and NO_2 was typically below 1%; a variation of the H_2 and NO_2 partial flows by a factor of 5 had no influence on the results. The temperature close to the laser beam was measured with a thermocouple; the value obtained (300 K) ensured that heat released by the microwave discharge had no influence on the temperature in this region of the flow system. In addition, all volumetric flows and the total pressure—measured with a capacitance manometer (Baratron 10 mbar range)—in the cell were monitored during each experiment and stored on the computer. The standard deviations of these values were less than 1% for all series of measurements.

The fluorescence was recorded at 90° relative to the laser beam, using two different detection systems. One detection system allowed the spectral resolution of individual lines in the OH (A–X) band; the other system, which was used as a reference, detected the fluorescence without spectral resolution.

For the spectrally resolved fluorescence system, a $f/3.75$ quartz lens focused the LIF signal on the entrance slit of a 640 mm grating spectrometer (Jobin Yvon HR640). A slit width and height of 50 μm and 2 mm, respectively, was chosen resulting in a 3.5 cm^{-1} bandwidth (FWHM). The signal was recorded by a photomultiplier (Valvo XP2020Q) and processed by a gated boxcar integrator (Stanford Research Systems SR 250) for the registration of fluorescence spectra, or by a 400 MHz transient digitizer (Tektronix 7912AD) for the measurement of time-resolved fluorescence signals. Between 300 and 6000 shots were averaged for the evaluation of one time-dependent state population. For the measurements of fluorescence spectra 30 shots were internally averaged by the boxcar integrator. The spectral resolution of the detection system allows single-line observation of the $P_2(1')$, $Q_1(1,1')$, $P_1(2)$, $O_2(4)$, $S_1(1)$, $P_2(4,4')$, $O_2(5)$, $R_2(3)$, $P_1(5)$, $R_2(4)$, and $Q_1(5,5')$ lines in the A–X, 0–0 band of OH. The above nomenclature used to designate the lines is that of Dieke and Crosswhite.[41] The center of the line positions was checked before and after each series of measurements. Calibrated filters with transmissions between 0.05% and 50% ensured that the maxima of the intensities were approximately equal for all time-dependent single-line measurements.

The broadband reference system allowed corrections which were necessary due to small changes in the laser pulse energy, the wavelength of the laser, and the efficiency of the OH production. The measurements were discarded if the deviation in the reference signal exceeded 15%. The reference system consisted of a $f/1$ quartz lens, a spectral cutoff filter (Schott WG 320), a photomultiplier (RCA 1P28A) and a gated boxcar integrator (Stanford Research Systems SR 250). Stray light generated by the laser beam was suppressed by the cutoff filter and the time gate of the integrator; the gate width and its delay relative to the laser pulse were typically 100 and 150 ns, respectively. The fluorescence signals from both detection systems were stored simultaneously on a PDP 11/23 computer.

III. METHOD OF DATA ANALYSIS

All relevant processes for the determination of state-to-state energy transfer coefficients within the ($A\ ^2\Sigma^+$, $v'=0$) state of the OH radical are illustrated in Fig. 1. Each RET coefficient is evaluated from a pair of temporal evolutions of LIF signals, originating from the laser-pumped state i and a final state f populated by inelastic collisions. It is essential for our method that only one specific level i is initially excited by the laser. The way of analyzing the data is, in general, applicable to all experiments which probe relative number densities of single states within a vibrational manifold, with a time resolution sufficient to resolve the increase in the number density of a collisionally populated state. For example, this method is, in principle, applicable to evaluate RET coefficients of vibrationally excited molecules by pump/probe techniques.

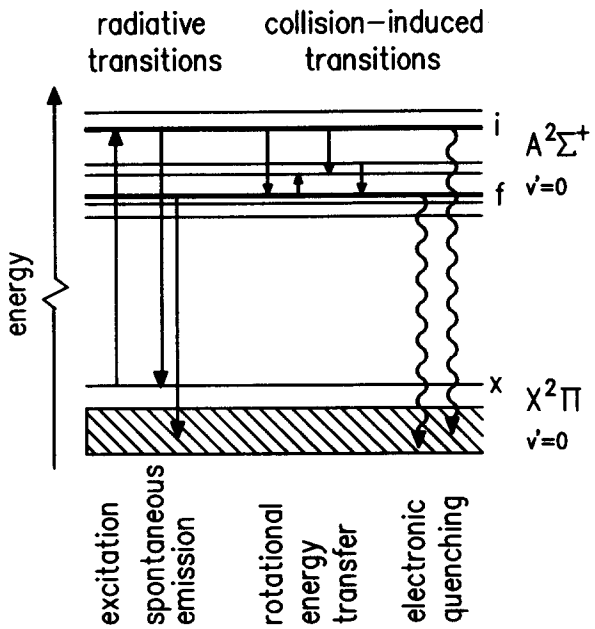

FIG. 1. Energy level scheme for OH, indicating the relevant radiative and collision-induced transitions.

The time-dependent populations of the collisionally populated levels within the OH (A, $v'=0$) state can be described by rate equations of the form

$$\frac{dN_f}{dt}=N_C\Big(N_i k_{if}+\sum_{j\neq i,f} N_j k_{jf}\Big) - N_f\Big[1/\tau_f+N_C\Big(k_f+\sum_{j\neq f} k_{fj}\Big)\Big], \quad (1)$$

with N_C being the number density of the collider/molecule cm^{-3}, N_i,N_j, and N_f the state-specific number density of OH/molecule cm^{-3}, τ_f, the state specific radiative lifetime/s, and k, the kinetic rate coefficient/cm^3 molecule^{-1} s^{-1}. (RET coefficients are denoted by two subscripts, coefficients with one subscript correspond to electronic quenching.)

Under our experimental conditions vibrational relaxation can be neglected. However, when necessary, a term for vibrational relaxation, analogous to that for electronic quenching, can be added. In the rate equations the subscripts i, f, and j indicate specific levels within the excited OH (A, $v'=0$) manifold. The subscript C refers to the collision partner, in this study He or Ar. Because the A state of the OH radical has $^2\Sigma^+$ structure, each subscript i, f, and j denotes a fine structure level, where within a Hund's case (b) representation[42] the total angular momentum **J** is defined by the vector addition of the rotational angular momentum **K** and the spin **S**. This means that the rate coefficients k_{if} describe collision-induced transitions which are inelastic in **K** and/or **J**.

For simplicity, the indices denoting the individual levels are ordered by the energy of the rotational states. For example, the indices 1, 2, 3, and 11 correspond to the levels

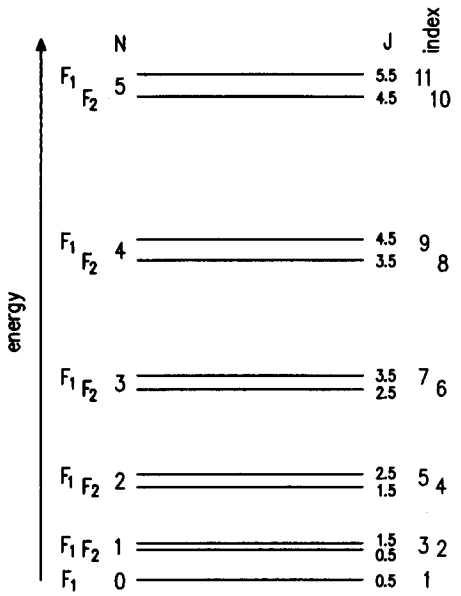

FIG. 2. The rotational level structure in the $A\ ^2\Sigma^+$, $v'=0$ state of OH. The splitting of the doublet components is exaggerated by a factor of 10.

$F_1(0)$, $F_2(1)$, $F_1(1)$, and $F_1(5)$, respectively. In other words, all odd subscripts represent F_1 levels, whereas all even subscripts represent F_2 levels. From a given subscript j the rotational quantum number N is obtained as $N=(j-1)/2$ for odd j and as $N=j/2$ for even j, respectively. The energy levels and the different notations are shown in Fig. 2.

To uncouple the rate equations, we neglect—to a first approximation—all transitions due to multiple collisions. As a result, level f can only be populated through a collision-induced transition originating from the laser-excited state i. We can thus rewrite Eq. (1) to give

$$\frac{dN_f}{dt}=N_C N_i k_{if}^s - N_f/\tau_f. \tag{2}$$

The superscript s of k_{if}^s indicates that this rate coefficient is derived by introducing the "single-collision approximation." The validity of this assumption will be discussed and demonstrated below.

Integration and rearrangement of Eq. (2) leads to the following equation for k_{if}^s:

$$k_{if}^s=\left(N_f^e - N_f^0 + 1/\tau_f \int_{t_0}^{t_e} N_f\, dt\right) \times \left(N_C \int_{t_0}^{t_e} N_i\, dt\right)^{-1}. \tag{3}$$

The integration is performed from t_0, the starting time of the laser pulse, to t_e, the end of the observation time. N_f^0 and N_f^e denote the OH number densities in state f at t_0 and t_e. In the following the behavior of k_{if}^s as a function of (t_e-t_0) and N_C will be discussed.

It is clear from the single-collision approximation itself, that the values of k_{if}^s, obtained by using the single-collision approximation [Eq. (3)], will approach the true coefficient k_{if} as the collision probability is reduced. In other words, it is possible to calculate k_{if} by extrapolating k_{if}^s to the limit of "zero-collision probability." In the experiments, the collision probability can be reduced by lowering the pressure of the collision gas—represented by N_C in Eq. (3)—or by limiting the observation time to small values of t_e. For a given pressure the best approximation of k_{if}^s to k_{if} is given by

$$k_{if}=\lim_{t_e\to t_0} k_{if}^s. \tag{4}$$

For sufficiently low pressures, this limit can be determined by calculating the axis intercept of a linear least squares fit of k_{if}^s vs (t_e-t_0).[40]

For the determination of k_{if}^s, it is not necessary to know the absolute values of the state-specific populations, since only a ratio of functions containing the populations—$f(N_f)/f(N_i)$—enters Eq. (3). The relative populations are calculated from the single-line LIF signals I_{jx}, using

$$N_j=C\frac{I_{jx}}{A_{jx}}, \tag{5}$$

where C comprises the observation volume, the solid angle, and the efficiency of the detection. The A_{jx} are Einstein coefficients for spontaneous emission. The subscript x refers to a rovibrational level of the electronic ground state; the possible values of x are determined by the selection rules for spontaneous emission. According to Eq. (5) the intensities of all fluorescence lines originating from a given level j scale with A_{jx} if C is assumed to be constant, independent of the wavelength. Measurements of fluorescence intensities were used to validate the assumption that C is a constant for the wavelength region used in the experiments. An example of such a measurement is given in Sec. IV A. The values of the Einstein coefficients for spontaneous emission[30] and the natural lifetimes[43] necessary for the data analysis were taken from the literature.

To demonstrate the feasibility of the data analysis procedure and to show its sensitivity to uncertainties in the radiative lifetime, model calculations were performed by numerical integration of the rate equations. The model consisted of 2 levels to describe the X state of OH and 11 levels to describe the A state. One level of the X state corresponded to the level which is coupled to the excited level i by the laser, the other represented all other rotational states of the electronic ground state. The temporal shape of the laser pulse and the probabilities for stimulated absorption and emission were chosen to fit typical experimental conditions. The rate coefficient for electronic quenching,[44] assumed to be level independent, was set to $10^{-12}/\mathrm{cm^3\ molecule^{-1}\ s^{-1}}$; the radiative lifetimes were taken from the literature.[43] The RET coefficients themselves were taken from quantum scattering calculations.[34] The number density of He was varied by a factor of 20, corresponding to pressures between 0.5 and 10 mbar.

Figure 3 shows results of these calculations and illustrates the data analysis procedure. In the upper part of this figure temporal evolutions for two state-specific OH populations (N_8 and N_{10}) are plotted for three different pressures. From these number densities the RET coefficients

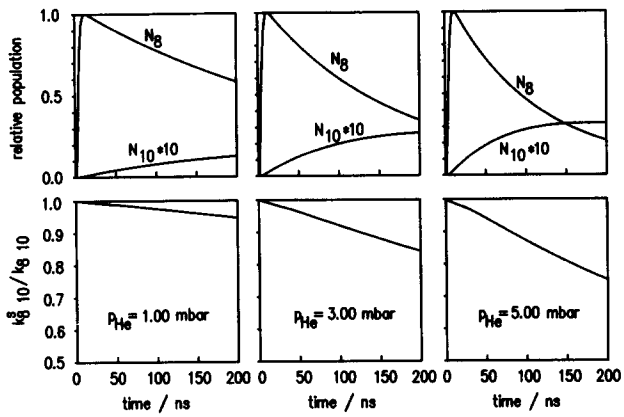

FIG. 3. Upper row: results from RET model calculations with He as collision partner for three different pressures. The number densities for the laser-excited state N_8 and a collisionally populated state N_{10} (multiplied by 10) are plotted. The values are normalized to the respective maxima of N_8. Lower row: data analysis using the calculated state populations. The rate coefficient $k^s_{8\,10}$ [calculated using Eq. (3)] is normalized to the true coefficient $k_{8\,10}$ used for the model calculation.

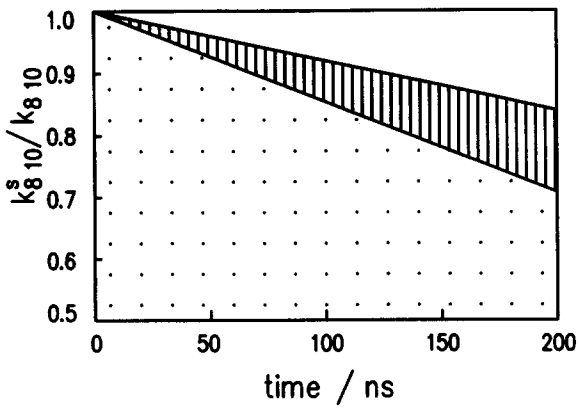

FIG. 4. Data analysis using the calculated populations shown in the middle of the upper row in Fig. 3. This figure is an enlargement of the plot shown in the middle of the lower row in Fig. 3. The dotted area corresponds to the contribution to $k^s_{8\,10}$ which is sensitive to the population difference $(N^e_{10} - N^0_{10})$. The shaded area corresponds to the contribution to $k^s_{8\,10}$ which is sensitive to the natural lifetime τ_{10}; compare Eq. (3) and detailed discussion in the text.

for the $8 \rightarrow 10$ transition are calculated in the single-collision approximation [Eq. (3)]. The resulting $k^s_{8\,10}$, normalized to the "true" $k_{8\,10}$ used for the model calculations, are shown in the lower part of Fig. 3. These plots demonstrate that k_{if} can be calculated as axis intercept of a linear regression of k^s_{if} vs time. The fact that k^s_{if} is a function of time reflects directly the breakdown of the single-collision approximation. The model calculations were applied to estimate the sensitivity of the data analysis to the time interval for the linear regression. In case of t_0 as the starting time of the laser pulse and t_e chosen to cut off the region where $k^s_{if}(t)$ behaves nonlinearly, the deviation of the k_{if} determined by the axis intercept from the true k_{if} used in the model calculation was below 2% for all pressures and transitions. A more detailed discussion of the assumptions that have to be observed in order to evaluate k_{if} accurately from k^s_{if} is given elsewhere.[40]

Figure 4 illustrates the insensitivity of our method to an uncertainty in the radiative lifetime τ_f. Equation (3) can be understood as composed of two additive terms, the first one involving the population difference $(N^e_f - N^0_f)$, the second one being influenced by τ_f. The dotted area in Fig. 4 represents the contribution of the first term, the shaded area corresponds to the contribution of the second term of k^s_{if}. Figure 4 demonstrates that an error in τ_f influences only the slope, but not the axis intercept of the k^s_{if} vs time plot. Therefore an error in τ_f has no effect on k_{if} which is calculated according to Eq. (4). In general, this behavior is due to the fact that the second term of Eq. (3) vanishes in the limit of $t_e \rightarrow t_0$ if t_0 is chosen as the starting time of the laser pulse.[40] In other words, the value of k_{if} determined from Eq. (4) is sensitive to the increase of N_f [first term of Eq. (3)] but not to the integral over N_f [second term in Eq. (3)]. For this reason, t_0 has to be properly chosen so that N^0_f is zero. In the experiments, the noise in the LIF signal at t_0, the starting time of the laser pulse, is a problem; therefore the average of $I_{fx}(t)$ for all $t < t_0$ monitored on the transient digitizer was used as $I_{fx}(t_0)$ in the data analysis.

For the experimental determination of RET coefficients, relative populations of individual levels were calculated from LIF signals according to Eq. (5). The monochromator bandpass allowed equal transmission for the $Q_1(1')$ satellite and the $Q_1(1)$ line; therefore the population of the $F_2(1)$ level was calculated from the measured $Q_1(1,1')$ and $P_1(2)$ intensities. We examined this procedure in the case of the $S_1(1)$, $P_2(4, 4')$, and $O_2(5)$ lines where redundant information was available. The relative number density in the $F_1(5)$ level was calculated from the $R_2(4)$ and the $Q_1(5,5')$ signals when the $F_2(4)$ level was laser excited.

The method of data analysis described above is not adequate to measure the $k_{8\,4}$, $k_{10\,4}$, and $k_{10\,11}$ coefficients with our experimental system. For the coefficients with $F_2(2)$ as final state ($k_{8\,4}$ and $k_{10\,4}$) this is due to the fact that the $R_2(1)$ line—corresponding to the $F_2(2)$ state—is partially overlapped by the $Q_1(4,4')$ line. This interference is pronounced in cases where the population in $F_1(4)$ or $F_2(4)$ is high compared to the population in $F_2(2)$. The reason why $k_{10\,11}$ cannot be easily obtained is the following. For a time soon after the laser pulse has started, a calculation of the $F_1(5)$ population from the $Q_1(5,5')$ and $R_2(4)$ signals is inadequate because of the very high population of the laser-excited $F_2(5)$ state compared to the $F_1(5)$ state. Unfortunately, these coefficients are important to measure; particularly $k_{8\,4}$ for collisions with He and $k_{10\,11}$ for collisions with Ar, since scattering calculations[31,34] predict these coefficients to be the largest for the given initial state and collision partner. Therefore, these coefficients were determined from fluorescence spectra with a different data analysis procedure which is described below.

We have evaluated $k_{8\,4}$, $k_{10\,4}$, and $k_{10\,11}$ from fluorescence spectra which were recorded with a narrow temporal

gate at different delays relative to the laser pulse. Those spectra contain the information necessary to determine RET coefficients simultaneously for all transitions. This advantage of spectra—compared to time dependences of single lines—is diminished by the loss of time-dependent information for the individual populations.

To avoid sophisticated, iterative analysis procedures, the experimental conditions have to be chosen so that the single-collision approximation is applicable. In this limit, Eq. (3) is valid; however, now in contrast to the discussion above, t_0 and t_e correspond to the beginning and the end of the integrator gate. The evaluation of k^s_{if} according to Eq. (3) from a single fluorescence spectrum is difficult because one spectrum—obtained at a certain time or time interval—contains no information about N^0_f and N^e_f. To investigate this problem, the model calculations described above were applied. One result of these calculations is that the $(N^e_f - N^0_f)$ term in Eq. (3) cannot be neglected under conditions for which the single-collision approximation is valid. Another result from these calculations, illustrated in Fig. 3, is that for low pressures and small values of $(t_e - t_0)$, the increase in N_f is approximately linear and therefore $(N^e_f - N^0_f)$ is proportional to the integral over N_f. Assuming a linear increase in N_f and choosing the zero point of the time scale so that $N_f\,(t=0)$ is zero,

$$N^e_f - N^0_f = \left(2\int_{t_0}^{t_e} N_f\,dt\right)(t_e + t_0)^{-1} \tag{6}$$

holds. Inserting Eq. (6) into Eq. (3) leads to

$$k^s_{if} = \int_{t_0}^{t_e} N_f\,dt\left(\frac{2}{t_e+t_0} + \frac{1}{\tau_f}\right)\left(N_C\int_{t_0}^{t_e} N_i\,dt\right)^{-1}. \tag{7}$$

With this equation, RET coefficients can be determined from a single LIF spectrum, if the necessary assumptions are observed in the experiment.

In addition, according to

$$k^s_{if} = k^s_{ij}\left(\int_{t_0}^{t_e} N_f\,dt\right)\left(\int_{t_0}^{t_e} N_j\,dt\right)^{-1}, \tag{8}$$

LIF spectra can be used to investigate the RET data for consistency. Here k^s_{ij} is a known coefficient, measured from time-resolved fluorescence signals. Equation (8) is derived from Eq. (7) assuming that the natural lifetime is level independent. This assumption is reasonable because the change in the lifetime of OH is less than 5% for the levels under investigation.[43]

We want to point out that for the determination of RET coefficients from LIF spectra, the systematic error is approximately 20%. For comparison, the systematic error for the method using time-resolved fluorescence signals is approximately 2%, as stated before. For this reason, only those coefficients are determined from spectra which cannot be obtained from time-resolved LIF signals with our experimental setup.

For the experimental determination of $k_{8\,4}$, $k_{10\,4}$, and $k_{10\,11}$, populations of the levels 1 corresponding to $F_1(0)$, 3 $[F_1(1)]$, 4 $[F_2(2)]$, 8 $[F_2(4)]$, 10 $[F_2(5)]$, and 11 $[F_1(5)]$ were evaluated from LIF spectra. All permutations of j and f were used to calculate as many coefficients as possible from Eqs. (7) and (8).

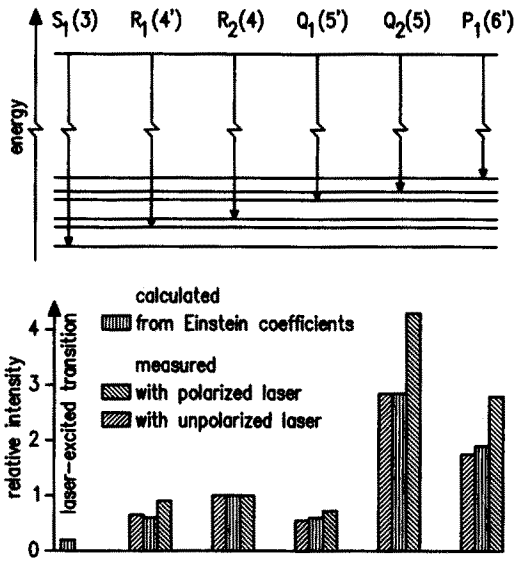

FIG. 5. Upper part: energy level scheme for the OH $(A$–$X)$ fluorescence lines originating from the $F_2(4)$ level. Lower part: relative intensities for these lines evaluated from LIF spectra measured with a prompt gate of 10 ns width at 1 mbar He. Also shown in this figure are the fluorescence intensities calculated from the Einstein coefficients for spontaneous emission (Ref. 30). The intensities are normalized to the respective $R_2(3)$ intensities.

IV. RESULTS AND DISCUSSION

A. Polarization

Figure 5 shows relative intensities of fluorescence lines originating from the $F_2(5)$ level in comparison with the isotropic Einstein coefficients for spontaneous emission.[30] All values are normalized to $R_2(4)$. The fluorescence signals were taken from spectra recorded with a gate of 10 ns width, without time delay relative to the laser pulse. The fluorescence of the $S_1(3)$ line was not measured because of interference from scattered laser light. The deviation of the observed intensities from the ratios of the Einstein coefficients is within the experimental uncertainty of typically 10% for the excitation with unpolarized light. Systematic deviations are observed if the exciting laser is not passed through a polarization scrambler. Thus a depolarizing element is required to obtain relative state populations from isotropic Einstein coefficients [Eq. (5)] under the experimental conditions used in this study. In addition, the assumption that C in Eq. (5) is a constant for the detection wavelength under consideration, is validated by the spectrum, taken after excitation with unpolarized light, where the intensities agree with those calculated from the Einstein coefficients.

B. State to state RET

The fluorescence spectra shown in Fig. 6 illustrate the effect of RET. With increasing delay, more and more lines originating from collisionally populated levels emerge, while the intensities of fluorescence lines originating from

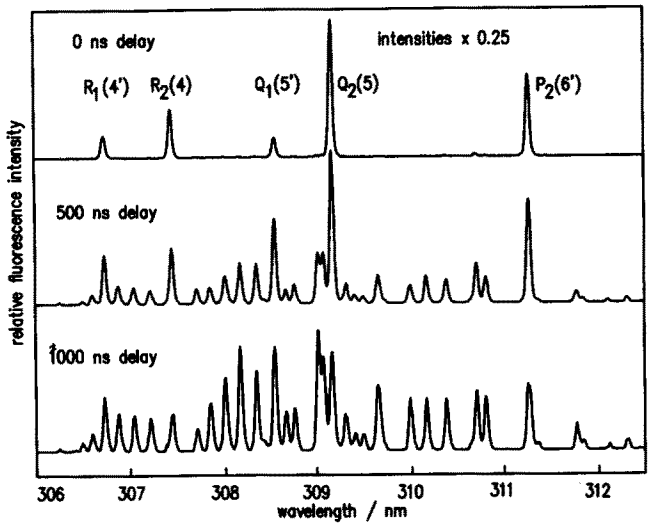

FIG. 6. Fluorescence spectra measured with a boxcar integrator (20 ns gate width). The time delays relative to the laser pulse are 0 ns (upper spectrum), 500 ns (spectrum in the middle), and 1 μs (lower spectrum), respectively. The intensities for the upper spectrum are multiplied by 0.25; all spectra are measured at 1 mbar He pressure.

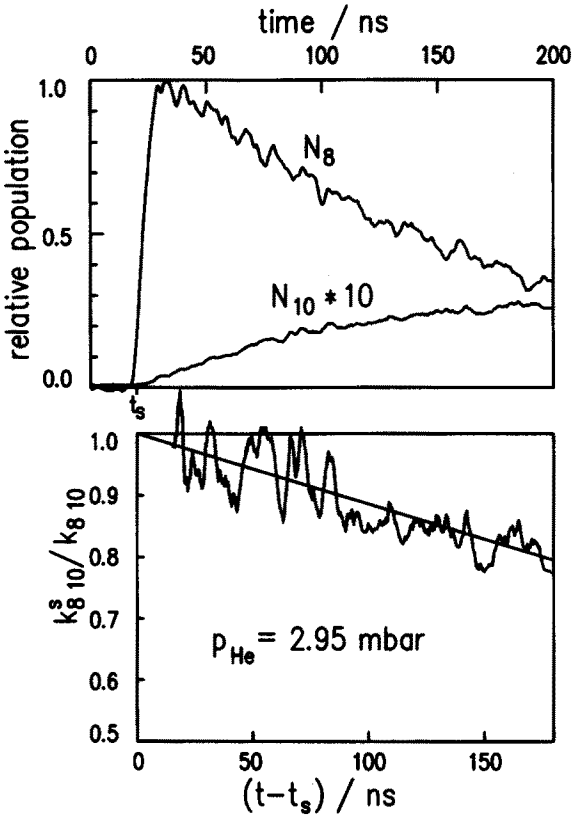

FIG. 7. Upper part: relative state-specific populations calculated from single-line LIF signals. The $F_2(4)$ state (N_8) is laser-excited; the population of $F_2(5)$ state (N_{10}) is multiplied by 10. Lower part: calculation of $k^s_{8\,10}$ according to Eq. (3) from the measured state-specific populations.

the initially pumped $F_2(5)$ level—$S_1(3)$, $R_1(4')$, $R_2(4)$, $Q_1(5')$, $Q_2(5)$, and $P_2(6)$—decrease. As described above, fluorescence spectra, with higher spectral resolution than the ones shown in Fig. 6, were used to estimate the $k_{8\,4}$, $k_{10\,4}$, and $k_{10\,11}$ coefficients according to Eqs. (7) and (8). These measurements were performed with a gate width of 50–150 ns and for time delays of 0–50 ns at rare gas pressures of 1–2 mbar. All other RET coefficients were evaluated from time-dependent relative state populations.

Figure 7 shows measured time-dependent LIF signals and the $k^s_{if}(t)$ derived from them according to Eq. (3). This figure should be compared to Fig. 3 to get an idea of the accuracy of the model calculations. The individual RET coefficients for He and Ar as collision partner are listed in Table I and II, respectively. The listed values are averages over 6–10 independent measurements at total pressures ranging from 1–6 mbar for He and from 1–5 mbar for Ar. Figure 8 shows that, in the pressure range under investigation, the determined rate coefficients do not depend on the pressure of the collision partner. This figure also indicates that our results correspond with microscopic reversibility within the experimental uncertainties. According to the relations of detailed balancing, additional RET coefficients, not given in Tables I and II, can be calculated.

In Fig. 9 the logarithm of the measured RET coefficients for OH (A) + He is plotted vs the energy transferred during the collision. This figure illustrates that a simple exponential gap fitting law is inappropriate to describe the measured coefficients. A detailed analysis of the validity of different fitting laws will be given in a future study. The coefficients for both initial states ($i = 8$, 10) behave qualitatively the same way. Surprisingly, the nearly isoenergetic transitions, $\Delta N = 0$ and $\Delta J = 1$ are not the most probable ones. The largest RET coefficients are obtained for $\Delta J = \Delta N = -2$. On average, the parity conserving transitions ($F_2 \rightarrow F_2$) are favored over the parity changing transitions ($F_2 \rightarrow F_1$). This trend is especially pronounced for small values of $|\Delta N|$ (see Fig. 10). A propensity to parity conservation was previously reported for the RET of OH (A, $v' = 0$) with Ar,[6,27] N_2,[6,27] and H_2.[6] The coefficients of Table I are in excellent agreement with

TABLE I. RET coefficients (10^{12}/cm^3 molecule^{-1} s^{-1}) for thermal collisions of OH ($A\,^2\Sigma^+$, $v' = 0$) with He at 300 K.[a]

		Initial state 8 $F_2(4)$	Initial state 10 $F_2(5)$
Final state			
1	$F_1(0)$	6.51±0.36	1.20±0.08
2	$F_2(1)$	2.45±0.32	2.64±0.14
3	$F_1(1)$	4.01±0.29	2.99±0.15
4	$F_2(2)$	19.9±1.2	3.08±0.41
5	$F_1(2)$	9.69±0.59	4.41±0.41
6	$F_2(3)$	9.51±0.82	15.1±0.9
7	$F_1(3)$	4.61±0.24	3.98±0.73
8	$F_2(4)$		9.75±0.76
9	$F_1(4)$	10.5±0.9	2.03±0.15
10	$F_2(5)$	5.90±0.59	
11	$F_1(5)$	1.06±0.07	5.53±0.69

[a]The listed uncertainties correspond to a statistical error of 1 standard deviation.

TABLE II. RET coefficients (10^{12}/cm^3 molecule^{-1} s^{-1}) for thermal collisions of OH ($A\,^2\Sigma^+$, $v'=0$) with Ar at 300 K.[a]

Final state		Initial state 8 $F_2(4)$	Initial state 10 $F_2(5)$
1	$F_1(0)$	4.69±0.39	3.02±0.34
2	$F_2(1)$	6.14±0.39	2.90±0.76
3	$F_1(1)$	8.38±0.36	5.38±0.29
4	$F_2(2)$	20.3±1.9	9.28±1.19
5	$F_1(2)$	19.6±0.8	14.5±2.8
6	$F_2(3)$	40.7±2.8	20.1±4.0
7	$F_1(3)$	30.6±1.7	16.4±2.5
8	$F_2(4)$		31.9±2.6
9	$F_1(4)$	80.3±1.8	27.0±3.2
10	$F_2(5)$	21.2±1.3	
11	$F_1(5)$	16.2±2.0	53.4±3.8

[a]The listed uncertainties correspond to a statistical error of 1 standard deviation.

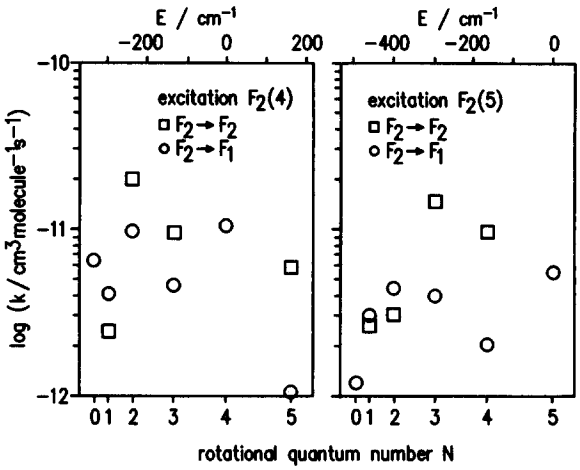

FIG. 9. Measured RET coefficients for thermal collisions of OH ($A\,^2\Sigma^+$, $v'=0$) with He at 300 K.

recent quantum scattering calculations.[34] These calculations confirm all trends mentioned above. A detailed discussion of the comparison between theory and experiment is given in Ref. 34.

For comparison, the OH–Ar RET coefficients are plotted in Fig. 11 on the same scale as for He. On average, the transition probabilities for Ar are about 3 times larger than those for He. The qualitative behavior of OH–Ar is very different from that of OH–He. In contrast to earlier studies[6,27] no significant propensity for parity conservation is found for OH–Ar (see Fig. 10). The most probable transitions are the nearly isoenergetic transitions with $\Delta N=0$ and $\Delta J=1$. The RET coefficients decrease with increasing energy transferred during the transition. The decrease is smoother for the initial level 8 [$F_2(4)$] than for the initial level 10 [$F_2(5)$]. A comparison of the experimental results with quantum scattering calculations utilizing an *ab initio* potential energy surface[31] is also possible for OH–Ar. Again, the agreement between theory and experiment is very good; a detailed discussion of this comparison is given in Ref. 31.

Although RET coefficients for OH (A, $v'=0$) + Ar have been previously reported by Lengel and Crosley[6] (LC), a quantitative comparison with this study is not directly possible. This is due to the fact that LC considered only transitions starting from the initial levels 3 and 9. A comparison becomes possible assuming that the individual coefficients obey the principle of microscopic reversibility. The $k_{3\,8}$ and $k_{9\,10}$ coefficients calculated from Table II, using the relations for detailed balancing, agree with those reported by LC within the experimental errors (see Table III). In contrast, $k_{9\,8}$ and $k_{3\,10}$, calculated from Table II, do not agree with the results of LC. Compared to our values, LC reported a lower value for $k_{9\,8}$ and a higher value for $k_{3\,10}$. Since $k_{9\,8}$ is the largest coefficient of all $k_{9\,f}$

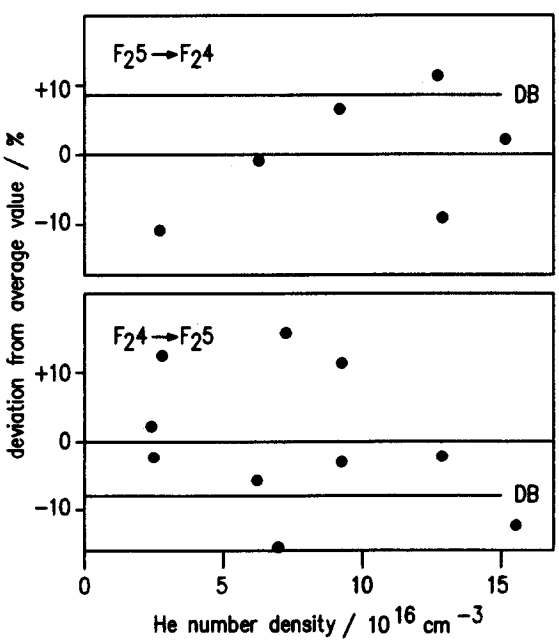

FIG. 8. Measured RET coefficients ($k_{8\,10}$ and $k_{10\,8}$/cm^3 molecule^{-1} s^{-1}) for 1–6 mbar He pressure. The average values are $k_{10\,8}=9.75\times10^{-12}$ cm^3 molecule^{-1} s^{-1} (upper row) and $k_{8\,10}=5.90\times10^{-12}$ cm^3 molecule^{-1} s^{-1}. The values marked by "DB" correspond to the relations for detailed balancing at a temperature of 300 K.

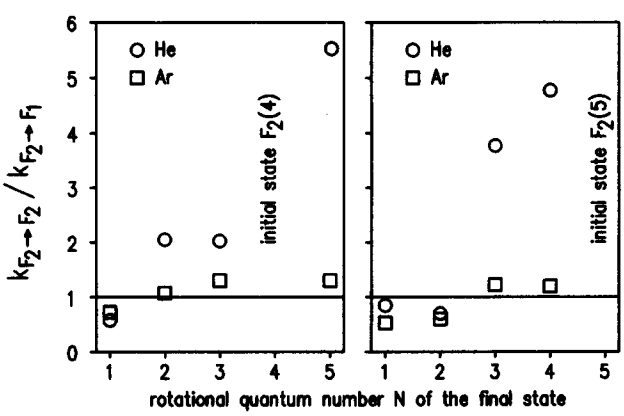

FIG. 10. Ratios of measured RET coefficients for a given ΔN. The coefficients for He as collider show a strong propensity for conserving the parity of OH.

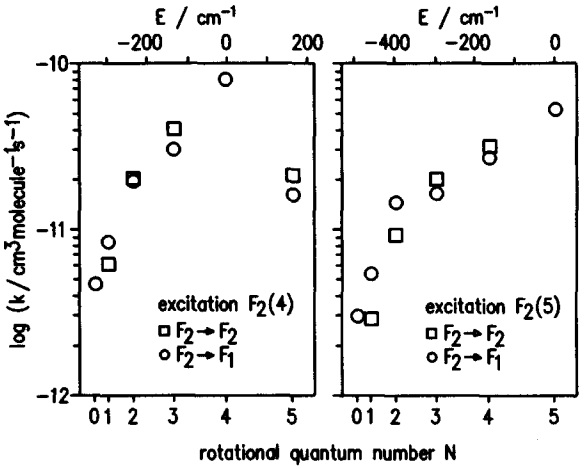

FIG. 11. Measured RET coefficients for thermal collisions of OH ($A\ ^2\Sigma^+$, $v' = 0$) with Ar at 300 K.

starting from initial level 9, and since $k_{3\,10}$ is an order of magnitude lower than the largest coefficient of all $k_{3\,f}$, the deviation could be due to an improper description of the multiple collision effects by LC. In general, the neglect of multiple collisions leads to an underestimation of large coefficients and to an overestimation of small coefficients. This explanation seems likely also in view that our results agree much better with the theoretical predictions[31] than those of LC. A comparison of both experimental data sets (LC and this study) with the calculated RET coefficients for OH (A) + Ar is given in Ref. 31.

The qualitatively different behavior of Ar and He which has been found in our experimental study is fully confirmed by theoretical investigations.[31,34] The difference in RET of OH–Ar and OH–He can be explained by a comparison of the calculated interaction potentials for the two systems. Reference 34 contains a detailed discussion of this comparison.

V. CONCLUSION

A method for the investigation of the state-to-state energy transfer within excited molecular states has been developed. The capability of the method has been demonstrated for thermal collisions of OH (A, $v' = 0$) with He and Ar, using a LIF excitation/detection scheme. The method is free of *a priori* assumptions concerning RET. This is important, since we are interested in a basic understanding of the collision dynamics involving the A state of the OH radical. In this context, a comparison of our experimental results with quantum scattering calculations, which is possible for OH (A) + He and Ar, is very helpful. The agreement between the calculated rate coefficients[31,34] and our measurements is very good. The difference in the qualitative trends of the RET coefficients for collisions with He compared to collisions with Ar is in accord with the predictions of theory.[31,34]

The OH (A) was chosen for this RET study because of the importance of the collision-induced energy transfer of OH for LIF measurements in combustion environments.[1,2]

TABLE III. RET coefficients (10^{12}/cm^3 molecule^{-1} s^{-1}) for thermal collisions of OH ($A\ ^2\Sigma^+$, $v' = 0$) with Ar at 300 K.

		Initial state	
		3	9
Final State		F_1	$F_1(4)$
8	$F_2(4)$	4.40 ± 0.43[a]	26.0 ± 1.0[a]
		5.7[b]	79.2[b]
		3.90[c]	99.9[c]
10	$F_2(5)$	4.40 ± 0.38[a]	12.8 ± 1.0[a]
		1.0[b]	7.0[b]
		1.40[c]	12.1[c]

[a]Experimental values taken from LC (Ref. 6).
[b]Calculated values taken from Ref. 31.
[c]Values obtained from Table II according to the principle of detailed balancing.

Our long-term goal is to build up a model that allows to judge the applicability of different LIF strategies under specific combustion conditions and to assist in the quantitative interpretation of LIF experiments. To this end, we have extended the available data base of RET coefficients for the flame relevant collision partners H_2O, CO_2, and N_2.[37] Further measurements, especially for the energetically lowest initial state $F_1(0)$ are in progress because this state is of particular importance for some dynamically based scaling laws.[39] The whole data will be used to examine the ability of common scaling and fitting laws[39] to describe the collision-induced RET of OH (A). In addition, RET coefficients for OH (A, $v' = 1$) will be measured, since excitation of this state for LIF measurements in combustion environments[38] has recently gained importance.

ACKNOWLEDGMENTS

The research described here is supported by the Research Association TECFLAM, Project 6.3. The authors are indebted to Professor Thomas Just for helpful discussions, to Dr. Annette Lawitzki and Dr. Timothy Griffin for assistance with some of the measurements, and to Dr. Alessandra Degli Esposti and Professor Hans-Joachim Werner for providing them with data of Ref. 31 prior to publication.

[1] A. C. Eckbreth, *Laser Diagnostics for Combustion Temperature and Species*, edited by A. K. Gupta and D. G. Lilley (Abacus, Cambridge, 1988).
[2] D. R. Crosley, J. Phys. Chem. **93**, 6273 (1989); K. Kohse-Höinghaus, Appl. Phys. B **50**, 441 (1990).
[3] I. J. Wysong, J. B. Jeffries, and D. R. Crosley, J. Chem. Phys. **92**, 5218 (1990).
[4] K. Bergmann and W. Demtröder, Z. Phys. **243**, 1 (1971); J. Phys. B **5**, 1386, 2098 (1972).
[5] R. B. Kurzel, J. I. Steinfeld, D. A. Hatzenbuhler, and G. E. Leroi, J. Chem. Phys. **55**, 4822 (1971); S. L. Dexheimer, M. Durand, T. A. Brunner, and D. E. Pritchard, *ibid.* **76**, 4996 (1982); H. Chun, H. Ruiping, and Z. Cunhao, Appl. Phys. B **41**, 251 (1986).
[6] R. K. Lengel and D. R. Crosley, J. Chem. Phys. **67**, 2085 (1977).
[7] T. A. Brunner, R. D. Driver, N. Smith, and D. E. Pritchard, Phys. Rev. Lett. **41**, 856 (1978); M. Wainger, I. Al-Agil, T. A. Brunner, A. W. Karp, N. Smith, and D. E. Pritchard, J. Chem. Phys. **71**, 1977 (1979); T. A. Brunner, R. D. Driver, N. Smith, and D. E. Pritchard, *ibid.* **70**, 4155 (1979); T. Brunner, N. Smith, and D. E. Pritchard, Chem. Phys.

Lett. **71**, 358 (1980); T. A. Brunner, N. Smith, A. W. Karp, and D. E. Pritchard, J. Chem. Phys. **74**, 3324 (1981).
[8] Ch. Ottinger and M. Schröder, J. Phys. B **13**, 4163 (1980); T. P. Scott, N. Smith, and D. E. Pritchard, J. Chem. Phys. **80**, 4841 (1984).
[9] J. Dufayard and O. Nédélec, Chem. Phys. **71**, 279 (1982); O. Nédélec and J. Dufayard, Chem. Phys. **105**, 371 (1986).
[10] M. Giroud and O. Nédélec, J. Chem. Phys. **77**, 3998 (1982).
[11] O. Nédélec and J. Dufayard, Chem. Phys. **84**, 167 (1984).
[12] M. Ferray, J. P. Visticot, and B. Sayer, J. Chem. Phys. **81**, 3009 (1984).
[13] C. Dufour, B. Pinchemel, M. Douay, J. Schamps, and M. H. Alexander, Chem. Phys. **98**, 315 (1985)
[14] S. J. Davis and K. W. Holtzclaw, J. Chem. Phys. **92**, 1661 (1990).
[15] J. J. Hinchen, Appl. Phys. Lett. **27**, 672 (1975); J. J. Hinchen and R. H. Hobbs, J. Chem. Phys. **65**, 2732 (1976).
[16] R. A. Copeland, D. J. Pearson, and F. F. Crim, Chem. Phys. Lett. **81**, 541 (1981); R. A. Copeland and F. F. Crim, J. Chem. Phys. **78**, 5551 (1983); *ibid.* **81**, 5819 (1984).
[17] A. S. Sudbø and M. M. T. Loy, Chem. Phys. Lett. **82**, 135 (1981); A. S. Sudbø and M. M. T. Loy, J. Chem. Phys. **76**, 3646 (1982).
[18] W. Meier, G. Ahlers, and H. Zacharias, J. Chem. Phys. **85**, 2599 (1986).
[19] R. L. Farrow and D. W. Chandler, J. Chem. Phys. **89**, 1994 (1988); J. Arnold, T. Dreier, and D. W. Chandler, Chem. Phys. **133**, 123 (1989).
[20] D. W. Chandler and R. L. Farrow, J. Chem. Phys. **85**, 810 (1986).
[21] F. Menard-Bourcin, T. Delaporte, and J. Menard, J. Chem. Phys. **84**, 201 (1986); E. A. Rohlfing, D. W. Chandler, and D. H. Parker, *ibid.* **87**, 5229 (1987).
[22] A. V. Smith and A. W. Johnson, Chem. Phys. Lett. **93**, 608 (1982); T. Imajo, K. Shibuya, and K. Obi, *ibid.* **137**, 139 (1987).
[23] B. K. Clark and I. M. Littlewood, Opt. Commun. **62**, 91 (1987).
[24] T. Carrington, J. Chem. Phys. **31**, 1418 (1959).
[25] M. Kaneko, Y. Mori, and I. Tanaka, J. Chem. Phys. **48**, 4468 (1968).
[26] K. H. Welge, S. V. Filseth, and J. Davenport, J. Chem. Phys. **53**, 502 (1970).
[27] D. Stepowski and M. J. Cottereau, J. Chem. Phys. **74**, 6674 (1981).
[28] R. P. Lucht, D. W. Sweeney, and N. M. Laurendeau, Appl. Opt. **25**, 4086 (1986).
[29] J. Burris, J. J. Butler, T. J. McGee and W. S. Heaps, Chem. Phys. **124**, 251 (1988).
[30] A. Goldman and J. R. Gillis, J. Quant. Spectrosc. Radiat. Transfer **25**, 111 (1981).
[31] A. Degli Esposti and H.-J. Werner, J. Chem. Phys. **93**, 3351 (1990).
[32] C. Chakravarty, D. C. Clary, A. Degli Esposti, and H.-J. Werner, J. Chem. Phys. **93**, 3367 (1990).
[33] W. Fawzi and M. C. Heaven, J. Chem. Phys. **89**, 7030 (1988); M. T. Berry, M. R. Brustein, and M. I. Lester, Chem. Phys. Lett. **153**, 17 (1988); M. T. Berry, M. R. Brustein, J. R. Adamo, and M. I. Lester, J. Phys. Chem. **92**, 5551 (1988).
[34] A. Jörg, A. Degli Esposti and H. -J. Werner, J. Chem. Phys. (submitted).
[35] A. Vegiri and S. C. Farantos, J. Phys. Chem. **92**, 2723 (1988).
[36] S. C. Farantos and A. Vegiri, J. Phys. Chem. **92**, 2719 (1988).
[37] A. Jörg, U. Meier, and K. Kohse-Höinghaus (to be published).
[38] A. Lawitzki, R. Tirgrath, U. Meier, K. Kohse-Höinghaus, A. Jörg, and Th. Just, *Proceedings of the Joint Meeting of German and Italian Sections of the Combustion Institute,* (The Combustion Institute, Sezione Italiana, Napoli, 1989); A. Lawitzki, I. Plath, W. Stricker, J. Bittner, U. Meier, and K. Kohse-Höinghaus, Appl. Phys. B **50**, 513 (1990); K. Kohse-Hönghaus, U. Meier, and B. Attal-Trétout, Appl. Opt. **29**, 1560 (1990).
[39] T. A. Brunner and D. Pritchard, Adv. Chem. Phys. **50**, 589 (1982); M. H. Alexander, J. Chem. Phys. **76**, 3637 (1982).
[40] A. Jörg, Ph.D. thesis, Universität Stuttgart (in preparation).
[41] G. H. Dieke and H. M. Crosswhite, J. Quant. Spectrosc. Radiat. Transfer **2**, 97 (1962).
[42] G. Herzberg, *Spectra of Diatomic Molecules,* 2nd ed. (Van Nostrand, Princeton, 1968).
[43] I. S. McDermid and J. B. Laudenslager, J. Chem. Phys. **76**, 1824 (1982).
[44] K. H. Becker and D. Haaks, Z. Naturforsch. Teil A **28**, 249 (1973), and references therein.